Laser and Particle Beams (2013), *31*, 457–464.
© Cambridge University Press, 2013 0263-0346/13 $20.00
doi:10.1017/S026303461300030X

Advances in the investigation of shock-induced reflectivity of porous carbon

DIMITRI BATANI,[1] STEFANO PALEARI,[2] TOMMASO VINCI,[3] ROBERTO BENOCCI,[1] KEISUKE SHIGEMORI,[4] YOICHIRO HIRONAKA,[4] TOSHIHIKO KADONO,[4] AND AKIYUKI SHIROSHITA[4]

[1]University Bordeaux, CEA, CNRS, CELIA (Centre Laser Intense at Applications), UMR 5107, Talence, France
[2]Dipartimento di Fisica G.Occhialini, Università di Milano Bicocca, Milan, Italy
[3]Laboratoire pour l'Utilisation des Lasers Intenses, UMR 7605 CNRS-CEA-Ecole Polytechnique-Paris VI, Palaiseau, France
[4]Institute of Laser Engineering, Osaka University, Suita City, Osaka, Japan

(Received 17 January 2013; Accepted 20 March 2013)

Abstract

We studied the behavior of porous carbon compressed by laser-generated shock waves. In particular, we developed a new design for targets, optimized for the investigation of carbon reflectivity at hundred-GPa pressures and eV/k temperatures. Specially designed "two-layer-two materials" targets, comprising porous carbon on transparent substrates, allowed the probing of carbon reflectivity and a quite accurate determination of the position in the P, T plane. This was achieved by the simultaneous measurement of shock breakout times, sample temperature (by optical pyrometry) and uid velocity. The experiments proved the new scheme is reliable and appropriate for reflectivity measurements of thermodynamical states lying out of the standard graphite or diamond hugoniot. An increase of reflectivity in carbon has been observed at 260 GPa and 14,000 K while no increase in reflectivity is found at 200 GPa and 20,000 K. We also discuss the role of numerical simulations in the optimization of target parameters and in clarifying shock dynamics.

Keywords: Laser induced shock-waves; Porous carbon; Reflectivity

1. INTRODUCTION

Carbon is a particularly interesting element due to the large variety of its different phases: solid phases like diamond and graphite at standard pressure and temperature, predicted super-diamond and metallic phases at high pressures, insulating, semi-mettallic and metallic liquid phases at high temperatures and pressures. The phase diagram in the lower region (under 50 GPa and for temperature below 6000 K) is relatively well established and the characteristics of the solid graphiteand diamond phases have been explored thoroughly. On the contrary, the liquid high-pressure and high-temperature state is poorly known due to the extreme conditions required to its study. The existence of metallic liquid carbon has been observed (Bundy *et al.*, 1996) and in the last two decades several studies (Thiel & Ree, 1993; Correa *et al.*, 2006; Grumbach & Martin, 1996; Gust, 1980; Wang *et al.*, 2005*a*; Romero & Mattson, 2007) speculated about the presence of a transition between liquid phases characterized by different conductivity at pressures above 80 GPa.

The phase diagram of carbon at high pressures and temperatures is very interesting for several domains of physics. In materials science, major issues include the predicted first-order phase transition in the liquid, the melting curve of graphite (Togaya, 1997), the exact behavior of the melting curve of diamond, and the nature of the liquid state (Grumbach & Martin, 1996; Wang *et al.*, 2005*b*). In inertial confinement fusion (ICF) research, compression efficiency and shock structure in fusion capsule critically depend on the thermodynamical properties of the materials of the capsule at extremely high-pressure conditions (Biener *et al.*, 2009), and this includes the use of carbon-based cone-guides in fast ignition research (Fujioka *et al.*, 2012). In planetology, the description of high-pressure phases is essential for developing realistic models of planets. For instance, carbon is a prime component (through methane and carbon dioxide) of giant planets such as Uranus and Neptune (Guillot, 1999). High pressures are thought to produce methane pyrolysis with a separation of the carbon phase and the possible formation of a diamond or metallic layer (Ross, 1981; Ancilotto *et al.*,). The high electrical conductivity layers generated in the

Address correspondence and reprint requests to: Dimitri Batani, Centre Lasers Intenses et Applications, Universit_e Bordeaux 1, Cours de la Liberation 351, 33405 Talence cedex, France. E-mail: batani@celia.u-bordeaux1.fr

https://doi.org/10.1017/S026303461300030X Published online by Cambridge University Press

mantle of these planets could be the source of the observed large magnetic fields (Nellis *et al.*, 1995).

Such interest has generated a large mass of experiments addressed to studying the equation of state of carbon, its phase transitions, and the physical characteristics of each phase (for instance electrical conductivity measured either directly or through the measurements of optical characteristics). In particular, experiments based on laser-driven shock compression has been used successfully in the last years, investigating extreme conditions (Ozaki *et al.*, 2004; Zvorkin *et al.*, 2004; Batani *et al.*, 2007; 2003; 2004; Hicks *et al.*, 2008; Bradley *et al.*, 2009), and stimulating further theoretical analyses (Eggert *et al.*, 2009; Wang *et al.*, 2005*a*; Das & Menon, 2009; Driver & Militzer, 2012; Nissim *et al.*, 2012).

In the experiments presented in this paper, we investigate a design for targets employed in laser induced shock-compression experiments, allowing the investigation of carbon state and carbon reflectivity at hundred-GPa pressures and eV/k temperatures. We used "two-layer–two materials" targets, comprising porous carbon on transparent substrates. The transparent substrate allows probing of carbon reflectivity (and also measuring fluid velocity by using a velocity interferometer system for any reflector (VISAR)) while porous carbon allows getting thermodynamical states lying out of the standard graphite or diamond hugoniot. In particular, we could reach the high-pressures and high-temperatures liquid phases. We could also determine the sample temperature by means of time resolved spectrography (Shigemori *et al.*, 2006). Shock dynamics has been studied using the hydrodynamical-radiative code MULTI, in order to tailor the characteristics of the targets and the coupling with the laser pulse. A great effort has been devoted to develop reliable simulations, adherent to the real physical situation, in particular, by employing an effective description of equation of state of porous carbon. Accurate simulations helped in the interpretation of the experimental outcomes and yielded important contributions to data analysis.

2. EXPERIMENTAL SETUP

The results discussed in the present paper were obtained in two series of experiments performed with the GEKKO/HIPER (High Intensity Plasma Experimental Research) system at the Institute of Laser Engineering (ILE), Osaka University.

The HIPER facility (Miyanaga *et al.*, 2001) is an irradiation system on the GEKKO XII (GXII) Nd glass laser system at ILE (Yamanaka, 1999). The facility provides one-dimensional compression by smoothed laser beams with short wavelength and high intensity. In the system, 12 beams of the GXII are bundled in an $F/3$ cone angle. The laser pulse has a wavelength of 527 nm (second harmonic, 2ω-beam), is approximately square in time with a full width at half maximum (FWHM) of 2.4 ns and a rise and fall time of 100 ps. Shock planarity is provided by the large focal spot of 1 mm diameter and KPP smoothing, as can be seen from the images recorded by the space-resolved pyrometry SOP reported in Figure 1. In the three shots that will be discussed below, the shock region is flat on a scale of 100 μm in shot 33083 and 250 μm in shots 33062 and 33065, while the time lag between the center and the wing of the shock wave is lass than 0.2 ns. The total energy of the laser pulse is measured with a calibrated calorimeter. For the experiments considered below, the peak laser intensities were 3.2×10^{12} W/cm^2 (shot 33083), 4.4×10^{12} W/cm^2 (shot 33062), and 9.8×10^{12} W/cm^2 (shot 33065) corresponding to total energies of 73.5 J, 101 J, and 225.7 J, respectively.

A schematic view of the experimental configuration is shown in Figure 2. Four diagnostics based on streak cameras with sub-nanosecond time resolution are used at the same time (Paleari *et al.*, 2013). Two of them collect the self-emission giving space-resolved and frequency-resolved emission intensity—a Streaked Optical Pyrometer (SOP) and a Streaked Spectrograph Optical Pyrometer (SSOP) (Shigemori *et al.*, 2006), respectively—giving information on shock planarity, time of shock breakout, preheating and emission time profile, while two VISARS recorded the speed and the reflectivity of the rear side of the target (Setchell, 2002).

The design of the targets is quite simple: a layer of porous carbon is deposited on a transparent substrate (either silica or lithium fluoride), the main laser beam hits the carbon and the rear surface is imaged by the diagnostics. This design has three advantages: first, the substrate prevents the carbon

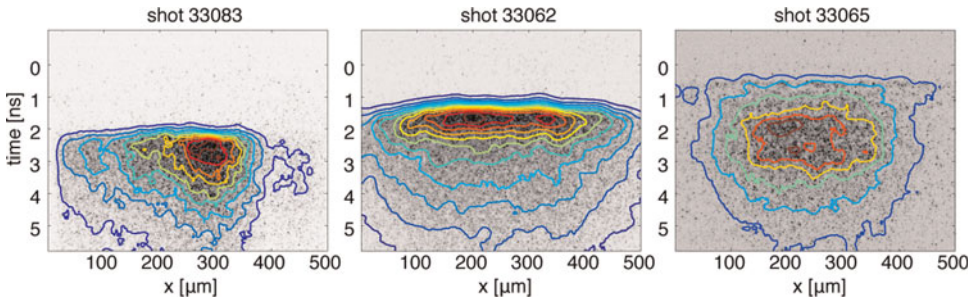

Fig. 1. (Color online) Shock planarity is provided by the large focal spot (1 mm diameter) and KPP smoothing. SOP images show intense shock fronts from 100 μm to 250 μm wide with a time lag of 0.2 ns between the center and the wings.

https://doi.org/10.1017/S026303461300030X Published online by Cambridge University Press

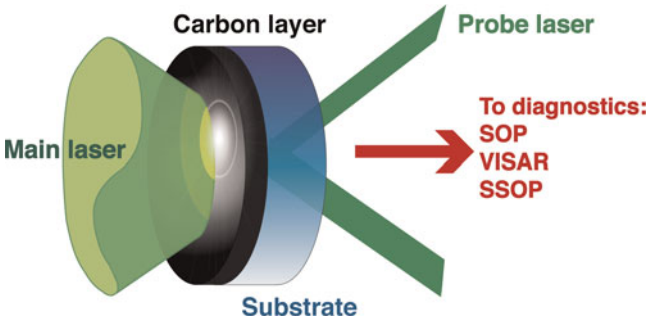

Fig. 2. (Color online) Experiment layout showing the "two-layer–two material" target design. The main laser pulse produces a shock wave propagating from the porous carbon through the substrate. The shock breakout in the transparent material is imaged by a streaked optical pyrometer (SOP) and a streaked spectrograph (SSOP) while a secondary laser reflects on the back of the target and the light is collected by two VISAR interferometers.

from releasing into vacuum after shock breakout, keeping the density high; second, it reflects the shock wave back due to its higher density, increasing the pressure; third, the interface between carbon and substrate is accessible to the optical diagnostics.

Two distinct series of targets have been produced at the Molecular Beam Laboratory (Università degli Studi di Milano, Italy) and at INFN National Laboratory, Frascati, Italy. In the first series, disks of fused silica (SiO_2—4 mm diameter and 100 μm thickness) were employed as substrates, with anti-reflective coatings for the wavelength of the probe laser on the bottom side. The carbon layer was deposited with supersonic cluster beam deposition (SCBD) technique (Milani *et al.*, 2001). The second series of targets was made with spray coating technique. Lithium fluoride (LiF) substrates of square shape (3×3 mm) and 300 μm thickness were used. Carbon density in both cases was about $0.5\,g/cm^3$ and thickness ranged between 5 and 50 μm. This density was selected for the interest in the shocked states below the carbon main hugoniot. In future experiments the density can be changed to obtain other points on the phase diagram.

3. SIMULATIONS AND RESULTS

The new target layout differs significantly from past approaches, in which the shock wave is generated in a dense material and then it propagates into the lower density carbon. In the present case, instead, the shock wave is generated right in the carbon layer and travels toward a denser material. For this reason, numerical simulations have been estensively employed throughout all the steps of the experimental campaign. First, simulations have been used to predict the experimental conditions, in order tooptimize the target design. Besides, during the experiment, they suggested the suitable laser energy shot by shot, according to the actual target characteristics. In the end, the most important contribution is that to the interpretation of the experimental findings. The simulations were performed with MULTI (Ramis *et al.*, 1988), a one-dimensional hydrodynamic radiative code. Thanks to the large ratio of focal spot diameter (initial shock size) to the carbon layer thickness, one-dimensional simulations do provide accurate predictions in our case. The actual time profile of the main laser, measured by the dedicated diagnostic, is included in the simulations and the target is accurately modeled. In particular, the thermodynamical properties of the materials are described by the equation of state (EoS), in the form of tables. SESAME (LA-UR-92-3407) tables were employed for the substrates, while for the porous carbon layer we adopted the quotidian equation of state model (QEOS) (More *et al.*, 1988) and the table was obtained by means of the computer program MPQEOS (Kemp & Meyer-ter Vehn, 1998). Owing to its high accuracy and the limited number of parameters required to build the EoS, the QEOS model revealed itself as a valuable choice in predicting the behavior of shocked materials (Paleari *et al.*, 2013). As a reasonable approximation, the porosity of the material is assumed to influence only the density and the elastic properties of the initial cold state. The final states at megabar pressures (1 megabar = 100 GPa) are assumed to be completely compacted, thus neglecting the influence of the porosity crush which is important only at the kilobar scale. Also, the effect of the melting on the EoS were not taken into account.

The study evidenced that when the shock wave reaches the interface between carbon and substrate, a shock wave propagates inside the substrate and a *re-shock* wave is reflected back into carbon, as predicted by the conservation laws. The transmitted wave lies on the main Hugoniot of the substrate and, therefore, the pressure is increased. Besides, a rarefaction wave appears when the reflected shock reaches the ablation front. The dynamics of this rarefaction wave is similar to the release of a shock in a low impedance medium, with the condition that the final pressure is the ablation pressure, determined by the laser intensity. As the laser intensity

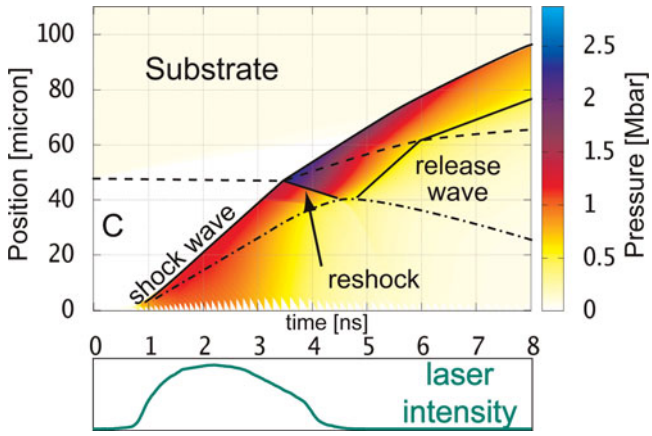

Fig. 3. (Color online) Shock dynamics in the case of thick carbon layer (≳25 μm). Pressure vs. space and time is plotted. The high pressure state is maintained for 1–2 ns, while, at the arrival of the rarefaction wave, pressure drop to zero.

https://doi.org/10.1017/S026303461300030X Published online by Cambridge University Press

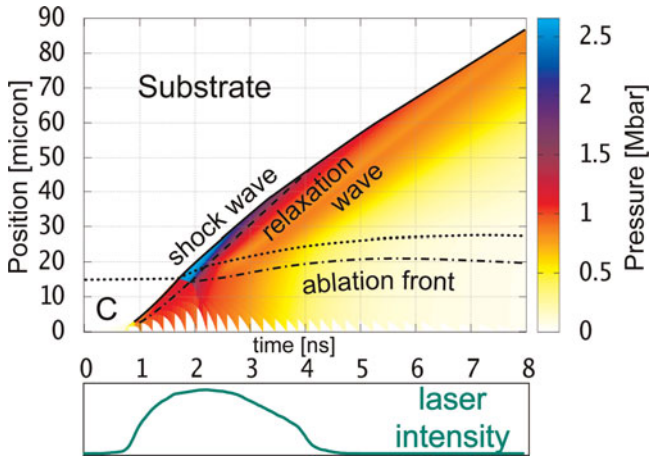

Fig. 4. (Color online) Shock dynamics in the case of thin carbon layer (≲25 μm). The high pressure state is maintained only for a fraction of ns. On the other hand, the rarefaction wave is generated when the laser pulse is at full intensity, thus the pressure of the release wave can still exceed 100 GPa.

varies rapidly in time, the pressure depends on the instant when the reflected shock reaches the ablation front, and eventually it approaches zero when the re-shock reaches the front side of the target after the end of the laser pulse.

Two typical regimes were identified, depending on the thickness of the carbon layer and its initial density. For a thick carbon layer (thickness ≳ 25 μm for a density of 0.5 g/cm^3), as shown in Figure 3, the re-shock state at the highest pressure is maintained for a time ranging between 1 and 2 ns, before the rarefaction wave drops the pressure to zero, like in the case of shock release in vacuum. On the other hand, for a thin carbon layer (thickness ≲25 μm for a density of 0.5 g/cm^3), the re-shock state is maintained only for less than 0.5 ns. In this case, however, the re-shock wave reaches the ablationfront when the laser pulse is close to the maximum intensity and the pressure does not drop to zero. Therefore, as can be seen in Figure 4, the pressure at the interface is bound to the ablation pressure and it follows the laser intensity profile with a few hundreds ps delay.

From an experimental poin of view, the target layout here proposed proved to be reliable and appropriate for reflectivity measurements of thermodynamical states lying outside the standard graphite or diamond hugoniot. A drawback of the present scheme is the need of a transparent substrate that can withstand the peak pressure with no appreciable opacification or increase of reflectivity. Fused silica has a threshold value of 100 GPa (Hicks *et al.*, 2005), while in lithium fluoride it exceeds 300 GPa (Clérouin *et al.*, 2006).

Figure 5 summarizes the main results obtained in the experimental campaign. In each column, the top graph shows the intensity of the light collected by the VISAR diagnostic, calculated integrating over the central portion of the fringe pattern. The corresponding image is shown in color scale, with the fringes evidenced by red lines. The last plot at the bottom compares the temperatures predicted by the MULTI simulation, that estimated from the SSOP image—the *spectral temperature*—and that from SOP diagnostic—the *brightness temperature*. Due to the finite size of the spectrograph slit and the image smoothing, employed to reduce

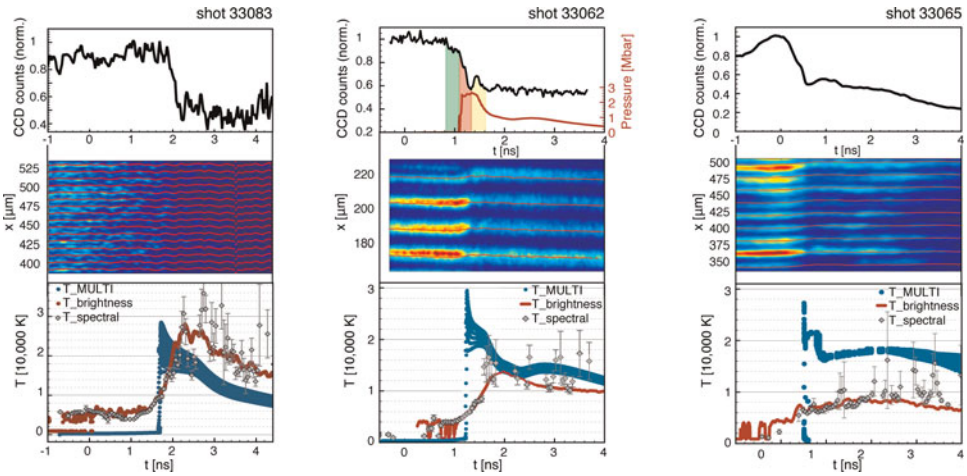

Fig. 5. (Color online) Graphical resume of the main experimental outcomes. In each of the three columns, the first plot on top shows the light reflected back from the target. The reflectivity is integrated on the central portion of the VISAR images, averaging out the fringe intensities. The corresponding images are displayed immediately below, with the fringe pattern evidenced by red lines. At the bottom, the plots present the spectral temperature calculated from the SSOP images, the brightness temperature from the SOP diagnostic, and the temperature predicted by the MULTI simulations. Due to the finite size of the spectrograph slit and the image smoothing, the time resolution of the experimental spectra is reduced to about 1 ns and the time profiles are rounded out. Simulations otherwise predict a very sharp step. As reported in the text, in the first shot from the left (no. 33083) the maximum pressure was about 200 Gpa and no increase in reflectivity was observed. In the middle, the most interesting shot (no. 33062) shows a reflectivity peak (shaded in yellow) after breakout (shaded in red), vanishing as pressure drops. The pressure predicted by simulations is plotted in red. On the right, an intense shot (no. 33065) produced a reflective shock front propagating into the SiO_2 substrate.

https://doi.org/10.1017/S026303461300030X Published online by Cambridge University Press

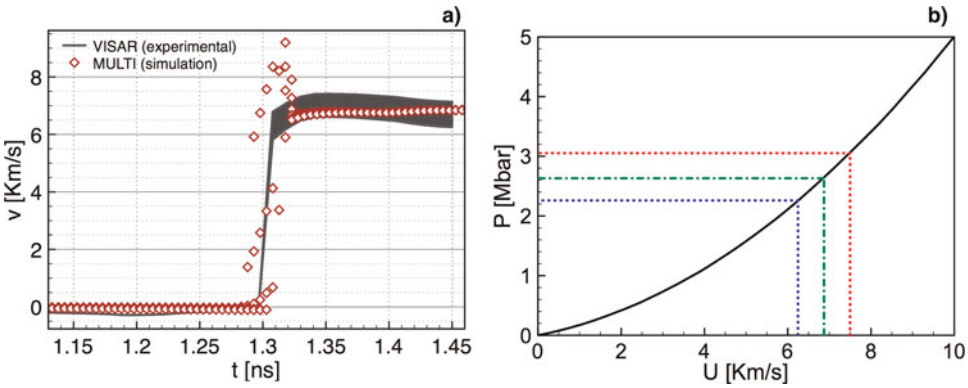

Fig. 6. (Color online) Hydrodynamic and equation of state relationships connect fluid velocity U with pressure P at a shock discontinuity. As the shocked carbon surface proceeds at the same speed of the compressed LiF substrate and the pressure is continuous across the interface, the measurement of the speed of the carbon surface yields the pressure, knowing the shock polar of LiF. The graph on the left shows the interface velocity calculated from fringe shift recorded by VISAR; higher and lower bounds are given; one fringe jump is considered at breakout. The presence of the window material and the change of its index of refraction under compression has been considered (Setchell, 2002; Clérouin *et al.*, 2006). On the right, lithium fluoride shock polar is plotted on the P-U plane; according to the VISAR, the fluid velocity is 6.8 ± 0.7 Km/s, thus the relation yields $P = 2.6 \pm 0.4$ Mbar (260 ± 40 GPa), as shown graphically on the right.

the noise, the time resolution of the experimental spectra is reduced to about 1 ns, smoothing the time profiles. Numerical simulations predict sharp steps instead. The targets with fused silica substrates did not provide useful data on carbon because pressure exceeded the threshold value (Fig. 5, right column). In the case of lithium fluoride substrates, opacification or increase of reflectivity of the window has been observed in high intensity shots, as well. At low laser intensities the reflectivity decreases at shock breakout (Fig. 5, left column), while at intermediate intensities it was possible to observe a sharp increase in reflectivity of the carbon (Fig. 5, center column). This is thought to be a clear signature of a reflective phase in carbon. The sudden decrease of reflectivity can be easily related to the pressure drop due to the arrival of the relaxation wave at the interface, predicted by the simulations at $t = 1.6$ ns (see Fig. 4). In order to validate the simulation results, the interface velocity U was calculated from the fringe shift recorded by the VISAR. In addition, the pressure was calculated from the shock polar of LiF (see Fig. 6). The previous analysis and the simulations concur to assign to the enhanced reflectivity state a pressure of 260 ± 40 GPa and temperature of 14,000 ± 2,000 K. The experiments did not reveal any increase in reflectivity up to 200 GPa and 20,000 ± 5,000 K (values estimated for shot 33083).

For illustration purpose, shot 33065 (with SiO_2 substrate) is discussed briefly as it is representative of substrate metallization, that is not to be confused with an increase of carbon reflectivity. With reference to Figure 5, right column, a highly reflective surface is visible for about 3 ns after the shock breakout. The velocity of this surface, calculated from the fringe shift, is consistent with the shock velocity

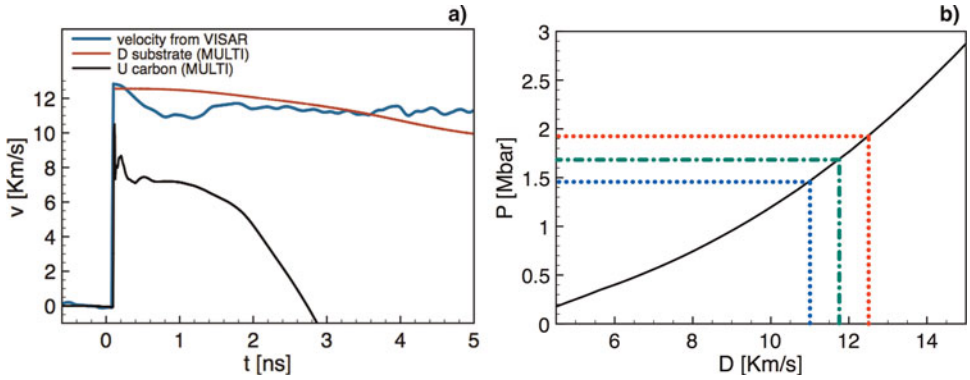

Fig. 7. (Color online) When the shock wave is strong enough to metallize the otherwise transparent substrate, the shock front becomes reflective. In shot 33065 the velocity calculated from VISAR is consistent with the shock velocity D predicted by MULTI simulations while the fluid velocity U is appreciably lower, as shown in the left plot. One fringe jump is considered at shock breakout. The Hugoniot curve for SiO_2 allows to obtain the pressure starting from D: to a velocity of 11.8 ± 0.7 Km/s corresponds a pressure of 1.7 ± 0.2 Mbar(170 ± 20GPa), as shown graphically on the right.

https://doi.org/10.1017/S026303461300030X Published online by Cambridge University Press

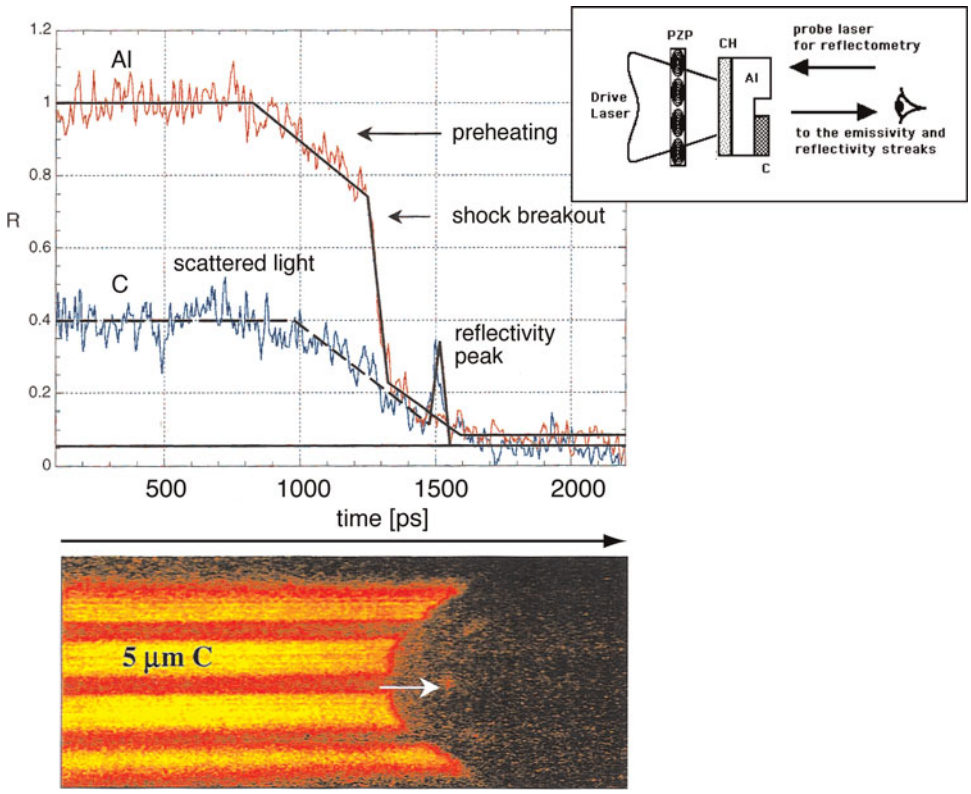

Fig. 8. (Color online) Increase in reflectivity in high-pressure carbon is confirmed also by a different laser induced shock-compression experiment, performed with porous carbon steps deposited on aluminum. The reflectivity of the rear target face, recorded with a streak camera and shown at the bottom, presents bright Al stripes and opaque carbon areas before shock arrival. At breakout the converse situation is observed, the aluminum reflectivity drops due to unloading of the material into vacuum while at the carbon sites a peak is observed (indicated by the white arrow). Above, carbon signal (in blue) is compared to the aluminum (in red).

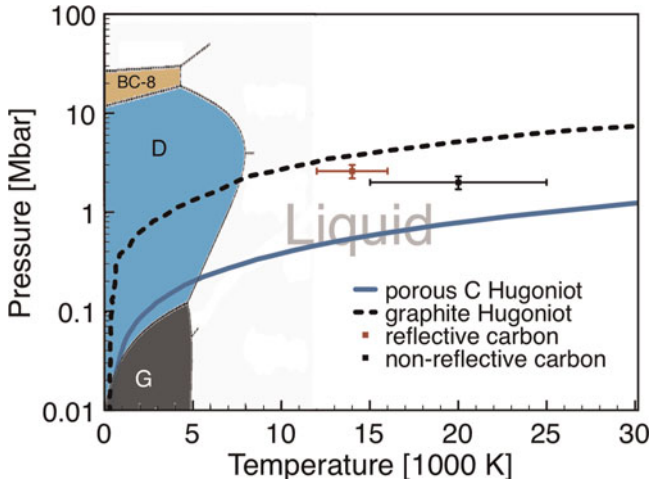

Fig. 9. (Color online) Phase diagram of carbon in the high pressure and temperature regime, after Grumbach & Martin (1996); the solid line (blue in the web version of this article) shows the porous carbon Hugoniot, the dashed black line indicates the graphite Hugoniot and the experimental points of reflective and non-reflective carbon are indicated by the squares; due to reflection of the shock at the interface, these points lie well above the Hugoniot; the regimes of stability of the graphite (G), diamond (D) and conductive BC-8 phases of carbon are indicated in gray, blue and yellow respectively.

D in the quartz substrate. This result allows us to estimate the pressure of the shock front from the Hugoniot curve of the SiO_2 (see Fig. 7). The resulting value of 170 ± 20 GPa is well above the metallization threshold of quartz (Hicks *et al.*, 2005), confirming the picture.

In addition, the increase in reflectivity in high-pressure carbon is confirmed by another experiment performed with a different setup (Tomasini, 2001). The targets contained carbon steps (with density $\rho_0 = 1.45$ g/cm^3) deposited on a 11 μm thick Al layer coated with a plastic ablator film (CH). The laser irradiates the CH/Al sheet and generates a shock wave that propagates into the carbon steps. The shock releases from the free surface of carbon into vacuum and the high pressure state is maintained only for a time of the order of 10–100 ps. Despite the short time scale of the phenomenon, an increase in reflectivity was measured. A typical outcome of this kind of experiment is reported in Figure 8. The brighter stripes are due to the high reflective Al substrate, while the dark lines are the opaque carbon steps. When the shock breaks out from the Al a signal drop is observed. On the contrary, when the shock breaks out from the carbon steps, a reflectivity peak is observed. Unfortunately the release of the shock at the free surface of carbon does not allow a reliable estimation of the actual state of

https://doi.org/10.1017/S026303461300030X Published online by Cambridge University Press

the unloading matter. Approximately, pressure and temperature ranged between 200 GPa and 800 GPa and between 10,000 K and 60,000 K, respectively.

4. CONCLUSIONS

We observed a clear signature of an increase of carbon reflectivity at 260 ± 40 GPa and 14,000 ± 2,000 K in the plane *P*, *T*. No increase in reflectivity is found up to 200 ± 40 GPa and 20,000 ± 5,000 K. These points could be used to estimate a line of metallization in a liquid state on the carbon phase diagram. This result is consistent with both earlier theoretical predictions (Grumbach & Martin, 1996) and recent theoretical estimation and experimental results (Eggert *et al.*, 2009; Correa *et al.*, 2006; Wang *et al.*, 2005*b*).

Figure 9 illustrates the up-to-date phase diagram of carbon as well as the porous carbon and the graphite Hugoniot curves and the experiment outcomes.

The limits of the carbon-on-transparent substrate design have been explored and a proof of principle of the whole experimental scheme has been obtained: the final state reached in compression can be varied tuning the carbon layer characteristics (initial density and thickness) and the laser intensity, with the possibility to determine the reflectivity of carbon and the position on the phase diagram, from the diagnostics. Also, the method is robust and ghost signals due to substrate metallization are easily individuated.

As a further improvement to overcome the limitation on the peak pressure imposed by the metallization of the transparent substrate, diamond could be used directly as the window material. The density and the thickness of the first porous carbon layer, as well as the laser pulse intensity, will be tailored to achieve the final thermodynamical state of interest. Then, any increase of reflectivity detected on the rear face would be a signature of the high conductive phase of carbon.

ACKNOWLEDGEMENTS

The authors are indebted and would like to thank P. Piseri of LGM (Laboratorio Getti Molecolari, Università degli Studi di Milano), S. Bellucci of LNF (Laboratori Nazionali di Frascati, Italy) and A. Mangione of ITA (Instituto Tecnologie Avanzate, Trapani) for the target manufacturing. The authors are also grateful to the Institute of Laser Engineering (ILE, Osaka University) for the fruitful collaboration. This work was supported by European Science Foundation (ESF) and by CNISM (Consorzio Nazionale Interuniversitario per le Scienze Fisiche della Materia).

REFERENCES

Ancilotto, F., Chiarotti, G. L., Scandolo, S. & Tosatti, E. (1997). Dissociation of methane into hydrocarbons at extreme (planetary) pressure and temperature. *Sci*. **275**, 1288–1290.

Batani, D., Dezulian, R., Redaelli, R., Benocci, R., Stabile, H., Canova, F., Desai, T., Lucchini, G., Krousky, E., Masek, K., Pfeifer, M., Skala, J., Dudzak, R., Rus, B., Ullschmied, J., Malka, V., Faure, J., Koenig, M., Limpouch, J., Nazarov, W., Pepler, D., Nagai, K., Norimatsu, T. & Nishimura, H. (2007). Recent experiments on the hydrodynamics of laser-produced plasmas conducted at the PALS laboratory. *Laser Part. Beams* **25**, 127–141.

Batani, D., Stabile, H., Ravasio, A., Lucchini, G., Strati, F., Ullschmied, J., Krousky, E., Skala, J., Kralikova, B., Pfeifer, M., Kadlec, C., Mocek, T., Präg, A., Nishimura, H., Ochi, Y., Kilpio, A., Shashkov, E., Stuchebrukhov, I., V, V. & I, K. (2003). Shock pressure induced by 0.44 μm laser radiation on aluminum targets. *Laser Part. Beams* **21**, 481–487.

Batani, D., Strati, F., Stabile, H., Tomasini, M., Lucchini, G., Ravasio, A., Koenig, M., Benuzzi-Mounaix, A., Nishimura, H., Ochi, Y., Ullschmied, J., Skala, J., Kralikova, B., Pfeifer, M., Kadlec, C., Mocek, T., Präg, A., Hall, T., Milani, P., Barborini, E. & Piseri, P. (2004). Hugoniot data for carbon at megabar pressures. *Phys. Rev. Lett*. **92**, 065503.

Biener, J., Ho, D. D., Wild, C., Woerner, E., Biener, M. M., El-dasher, B. S., Hicks, D. G., Eggert, J. H., Celliers, P. M., Collins, G. W., Teslich, N.E. J., Kozioziemski, B. J., Haan, S. W. & Hamza, A. V. (2009). Diamond spheres for inertial confinement fusion. *Nucl. Fusion* **49**, 112001.

Bradley, D. K., Eggert, J. H., Smith, R. F., Prisbrey, S. T., Hicks, D. G., Braun, D. G., Biener, J., Hamza, A. V., Rudd, R. E. & Collins, G. W. (2009). Diamond at 800 GPa. *Phys. Rev. Lett*. **102**, 075503.

Bundy, F., Bassett, W., Weathers, M., Hemley, R., Mao, H. & Goncharov, A. (1996). The pressure-temperature phase and transformation diagram for carbon; updated through 1994. *Carbon* **34**, 141–153.

Clérouin, J., Laudernet, Y., Recoules, V. & Mazevet, S. (2006). Ab initio study of optical properties of shock compressed silica and lithium fluoride. *J. Phys. A* **39**, 4387–4391.

Correa, A. A., Bonev, S. A. & Galli, G. (2006). Carbon under extreme conditions: Phase boundaries and electronic properties from _rst-principles theory. Proceedings of the Shock-induced carbon reflectivity National Academy of Sciences of the United States of America 103, 1204{1208.

Das, M. & Menon, S. (2009). Effects of bound electrons and radiation on shock Hugoniot. *Phys. Rev. B* **79**, 045126.

Driver, K. & Militzer, B. (2012). All-Electron Path Integral Monte Carlo Simulations of Warm Dense Matter: Application to Water and Carbon Plasmas. *Phys. Rev. Lett*. **108**, 115502.

Eggert, J. H., Hicks, D. G., Celliers, P. M., Bradley, D. K., McWilliams, R. S., Jeanloz, R., Miller, J. E., Boehly, T. R. & Collins, G. W. (2009). Melting temperature of diamond at ultrahigh pressure. *Nat. Phys*. **6**, 40–43.

Fujioka, S., Zhang, Z., Yamamoto, N., Ohira, S., Fujii, Y., Ishihara, K., Johzaki, T., Sunahara, A., Arikawa, Y., Shigemori, K., Hironaka, Y., Sakawa, Y., Nakata, Y., Kawanaka, J., Nagatomo, H., Shiraga, H., Miyanaga, N., Norimatsu, T., Nishimura, H. & Azechi, H. (2012). High-energy-density plasmas generation on GEKKO-LFEX laser facility for fast-ignition laser fusion studies and laboratory astrophysics. *Plasma Phys. Control. Fusion* **54**, 124042.

Grumbach, M. & Martin, R. (1996). Phase diagram of carbon at high pressures and temperatures. *Phys. Rev. B* **54**, 15730–15741.

Guillot, T. (1999). Interiors of Giant Planets Inside and Outside the Solar System. *Sci*. **286**, 72–77.

https://doi.org/10.1017/S026303461300030X Published online by Cambridge University Press

Gust, W. (1980). Phase transition and shock-compression parameters to 120 GPa for three types of graphite and for amorphous carbon. *Phys. Rev. B* **22**, 4744–4756.

Hicks, D. G., Boehly, T. R., Celliers, P. M., Bradley, D. K., Eggert, J. H., McWilliams, R. S., Jeanloz, R. & Collins, G. W. (2008). High-precision measurements of the diamond Hugoniot in and above the melt region. *Phys. Rev. B* **78**, 174102.

Hicks, D. G., Boehly, T. R., Celliers, P. M., Eggert, J. H., Vianello, E., Meyerhofer, D. D. & Collins, G. W. (2005). Shock compression of quartz in the high-pressure fluid regime. *Phys. Plasmas* **12**, 082702.

Kemp, A. J. & Meyer-ter Vehn, J. (1998). An equation of state code for hot dense matter, based on the QEOS description. *Nucl. Instr. Meth. Phys. Res*. **A 415**, 674–676.

LA-UR-92-3407 (1992). *Sesame: The lanl equation of state database*. Los Alamos: Los Alamos National Laboratory.

Milani, P., Piseri, P., Barborini, E., Podesta, A. & Lenardi, C. (2001). Cluster beam synthesis of nanostructured thin films. *J. Vacu. Sci. & Techn. A* **19**, 2025–2033.

Miyanaga, N., Nakatsuka, M., Azechi, H., Shiraga, H., Kanabe, T., Asahara, H., Daido, H., Fujita, H. & Fujita, K. (2001). The GEKKO XII-HIPER (High Intensity Plasma Experimental Research) System Relevant to Ignition Targets. 18th IAEA International Conference on Fusion Energy. Sorrento, Italy.

More, R. M., Warren, K. H., Young, D. A. & Zimmerman, G. B. (1988). A new quotidian equation of state (QEOS) for hot dense matter. *Phys. Fluids* **31**, 3059–3078.

Nellis, W., Ross, M. & Holmes, N. (1995). Temperature measurements of shock-compressed liquid hydrogen: Implications for the interior of Jupiter. *Sci*. **574**, 1249–1252.

Nissim, N., Eliezer, S., Werdiger, M. & Perelmutter, L. (2012). Approaching the cold curve in laser-driven shock wave experiment of a matter precompressed by a partially perforated diamond anvil. *Laser Part. Beams* **XX**, 1–7.

Ozaki, N., Tanaka, K. A., Ono, T., Shigemori, K., Nakai, M., Azechi, H., Yamanaka, T., Wakabayashi, K., Yoshida, M., Nagao, H. & Kondo, K. (2004). GEKKO/HIPER-driven shock waves and equation-of-state measurements at ultrahigh pressures. Phys. *Plasmas* **11**, 1600–1608.

Paleari, S., Batani, D., Vinci, T, Benocci, R., Shigemori, K., Hironaka, Y., Kadono, T., Shiroshita, A., Piseri, P., Bellucci, S., Mangione, A. & Aliverdiev, A. (2013). A new target design for laser shock-compression studies of carbon reflectivity in the megabar regime. *Euro. Phys. J. D* (in press).

Ramis, R., Schmalz, R. & Meyer-Ter-Vehn, J. (1988). MULTI - A computer code for one-dimensional multigroup radiation hydrodynamics. *Compu. Phys. Commun*. **49**, 475–505.

Romero, N. & Mattson, W. (2007). Density-functional calculation of the shock Hugoniot for diamond. *Phys. Rev. B* **76**, 214113.

Ross, M. (1981). The ice layer in Uranus and Neptune—diamonds in the sky? *Nat*. **292**, 435–436.

Setchell, R. E. (2002). Refractive index of sapphire at 532 nm under shock compression and release. *J. Appl. Phys*. **91**, 2833–2841.

Shigemori, K., Otani, K., Shiota, T., Azechi, H. & Mima, K. (2006). Shock pyrometry of laser-irradiated foils below 1 eV. *Jpn J. Appl. Phys*. **45**, 4224–4226.

Thiel, M. V. & Ree, F. (1993). High-pressure liquid-liquid phase change in carbon. *Phys. Rev. B* **48**, 3591–3599.

Togaya, M. (1997). Pressure dependences of the melting temperature of graphite and the electrical resistivity of liquid carbon. *Phys. Rev. Lett*. **79**, 2474–2477.

Tomasini, M. (2001). Studio dell'equazione di stato del ferro e del carbonio a pressioni dell'ordine dei Mbar generate da shock indotti da laser (English translation here). Master's thesis, Universitaé degliStudi di Milano.

Wang, Y., Liu, Z.-K., Chen, L.-Q., Burakovsky, L., Preston, D., Luo, W., Johansson, B. & Ahuja, R. (2005). Mean-field potential calculations of shock-compressed porous carbon. *Phys. Rev. B* **71**, 054110.

Wang, X., Scandolo, S., Car, R., Burakovsky, L., Preston, D., Luo, W., Johansson, B. & Ahuja, R. (2005). Carbon phase diagram from ab initio molecular dynamics. *Phys. Rev. Lett*. **95**, 185701.

Yamanaka, C. (1999). Inertial fusion research over the past 30 years. *Fusion Engin. Des*. **44**, 1–12.

Zvorykin, V., Bakaev, V., Lebo, I. & Sychugov, G. (2004). Hydrodynamics of plasma and shock waves generated by the high-power GARPUN KrF laser. *Laser Part. Beams* **22**, 51–57.

https://doi.org/10.1017/S026303461300030X Published online by Cambridge University Press